Quantitative Schlieren Diagnostic Applied to a Nitrogen Thermal Plasma Jet

Juan Camilo Chamorro, Leandro Prevosto, Ezequiel Cejas, and Héctor Kelly

***Abstract*— A quantitative interpretation of the schlieren technique applied to an atmospheric pressure, vortex-stabilized nitrogen thermal plasma jet generated in a direct-current nontransferred arc plasma torch (nitrogen gas flow rate of 25 NL/min, power level of 15 kW), discharging into ambient air is reported. A *Z*-type, two-mirror schlieren system was used in the research. The technique allowed inferring the temporally averaged values of the temperatures and densities of different species present in the plasma jet in a wide range of radial and axial distances. Deviations from kinetic equilibrium in the calculation of the plasma refractive index were accounted for, but maintaining the assumption of the local chemistry equilibrium. The influence of several assumptions on the accuracy of the measurements was considered. The results have shown that for a distance of 3.5-mm downstream from the nozzle exit, the kinetic equilibrium is realized (being both electron and gas temperatures values around 11 000 K), but noticeable deviation from kinetic equilibrium appears toward the jet border. On the other hand, a marked deviation from the kinetic equilibrium was found in the whole far field of the plasma jet, where the electron temperature remains still quite high (about 10 000 K at 30-mm downstream of the nozzle exit), well decoupled from the gas temperature (about 7000 K at the same distance). The obtained results are in reasonable good agreement with those previously reported by some of the authors by using a double floating probe method in the same plasma torch.**

***Index Terms*— Kinetic equilibrium, nontransferred arc plasma torch, schlieren technique, thermal plasma.**

I. Introduction

ATMOSPHERIC pressure thermal plasma jets generated in direct-current (dc) nontransferred arc plasma torches are used in a number of applications such as plasma surface modifications, spray coatings, material synthesis, and waste treatment [1]–[6].

Standard dc nontransferred (spraying-type) plasma torches operate with a central thoriated tungsten rod-type cathode and a water-cooled annular copper anode. Typical torch currents are in the range of a few hundred amperes. The plasma gas is injected into the gap between the two electrodes and serves to keep the arc root in a continuous motion over the surface of the anode. The torch voltage depends on the nature of the plasma gas and can vary between 20 and 30 V for atomic gases up to 100 V or more when operating with molecular gases. As the gas passes around the arc through the anode-nozzle constriction, it is heated and partially ionized, emerging from the nozzle as a thermal plasma jet with a specific enthalpy ranging between 5 and 35 MJ/kg. At the nozzle exit, the centerline value of the gas temperature is around 10 000–12 000 K (close to the electron one) and the velocity of a few hundred of meters per seconds [1]. However, a significant difference in the gas temperature fields (but little difference of the velocity fields) of the jet outflow could occur depending on the difference between the specific heat of the surrounding gas into which the plasma jet expands and that of the jet [7], [8]. The central core of the plasma jet is usually close to the local thermal equilibrium (LTE) at atmospheric pressure, but large deviations from the LTE can exist in the peripheral zone due to rapid particle diffusion [9].

The dynamics of a thermal plasma jet and its chemical state (as well as the interactions between the plasma and the injected material in the plasma-spraying application [4], [5]) are mainly controlled by the kinetic gas and electron temperatures; thus, a proper knowledge on the temperature of different species of the plasma becomes important not only for the plasma processing application, but also for understanding basic chemical mechanisms in thermal plasma jets.

Temperature measurements in nontransferred dc arc torches operated at atmospheric pressure have been mostly obtained using emission spectroscopic techniques (see [10]–[16]). All these works have assumed the validity of the LTE assumption to derive the temperature from the excited emitting levels population. It implies that collisions are the predominant mechanism and that temperature and concentration gradients are low, which is not the case in jet fringes. In these regions, diffusion plays an important role, especially for electrons, and temperatures deduced from atomic lines are generally overestimated [2]. Besides, plasma jets are often assumed axially symmetric (regardless of the method used in the inversion process [16]), but tomography procedures [17] were used as well. Temperature measurements of the plume of the plasma torch were also performed using the laser-scattering method [8]. This method has the advantages over the emission spectroscopic that it is only slightly affected by deviations from LTE. Other methods of temperature measurements that

Manuscript received December 14, 2017; revised May 7, 2018; accepted August 30, 2018. This work was supported in part by the Consejo Nacional de Ciencias y Tecnología under Grant PIP 11220120100453 and in part by Universidad Tecnológica Nacional under Grant PID 4626. The review of this paper was arranged by Senior Editor S. Portillo. *(Corresponding author: Juan Camilo Chamorro.)*

J. C. Chamorro, E. Cejas, and H. Kelly are with the Grupo de Descargas Eléctricas, Departamento Ing. Electromecánica, Universidad Tecnológica Nacional, Facultad Regional Venado Tuerto, Venado Tuerto 2600, Argentina (e-mail: jcchamorro@utp.edu.co).

L. Prevosto is with the Grupo de Descargas Eléctricas, Departamento Ing. Electromecánica, CONICET, Universidad Tecnológica Nacional, Facultad Regional Venado Tuerto, Venado Tuerto 2600, Argentina.

Color versions of one or more of the figures in this paper are available online at http://ieeexplore.ieee.org.

Digital Object Identifier 10.1109/TPS.2018.2869031

have been applied to plasma torches are the enthalpy [18] and Langmuir [19], [20] probe techniques. Enthalpy probe measurements are generally possible only at temperatures well below 10 000 K, and significantly perturb the plasma.

Refractive optical methods represent a versatile tool for performing nonintrusive, quantitative measurements in transparent media [21]. In particular, refractive techniques allow the investigation of the gas density distribution in transparent flows by measuring its index of refraction (or its spatial derivatives). These refractive techniques can be divided into two groups: the interference methods based on the difference in length of the light ray paths, and the methods based on the angular deflections of the light rays, such as shadowgraph and schlieren. The schlieren technique is based on the angular deflection undergone by a light ray when passing through a region characterized by refractive index non-homogeneities. In fluids, these non-homogeneities are generally caused by density or temperature variations; therefore, the measured optical data can be processed in order to gain information on such variables. An extensive description of the schlieren technique can be found elsewhere [22], [23].

Quantitative schlieren techniques have been used in the past to determine the gas temperature and plasma composition in atmospheric-pressure nonthermal plasma jets [24], [25], nanosecond repetitively pulsed discharges [26], flames [27], and thermal arcs [28]–[30].

In this paper, a quantitative interpretation of the schlieren technique applied to an atmospheric pressure, vortex-stabilized nitrogen thermal plasma jet generated in a dc nontransferred arc plasma torch discharging into ambient air is reported. The technique allowed inferring the temporally averaged values of the temperatures and densities of different species present in the plasma jet by processing the gray-level contrast values of a digital schlieren image recorded at the observation plane for a given position of a transverse knife-edge located at the exit focal plane of the optical system. To the best of the author's knowledge, a quantitative interpretation of the schlieren technique applied to a thermal plasma jets generated in nontransferred arc plasma torches is for the first time reported.

This paper is organized as follows. The experimental arrangement and the techniques are described in Section II. The experimental results and its discussion are given in Section III. The conclusion is summarized in Section IV.

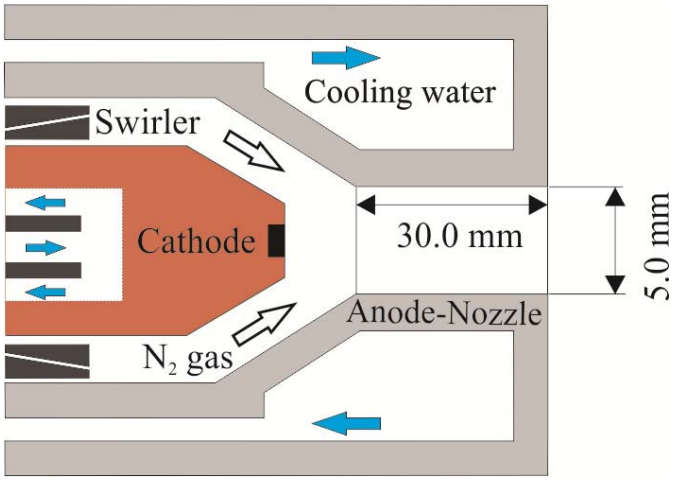

Fig. 1. Schematic of the nontransferred arc torch used in the experiment.

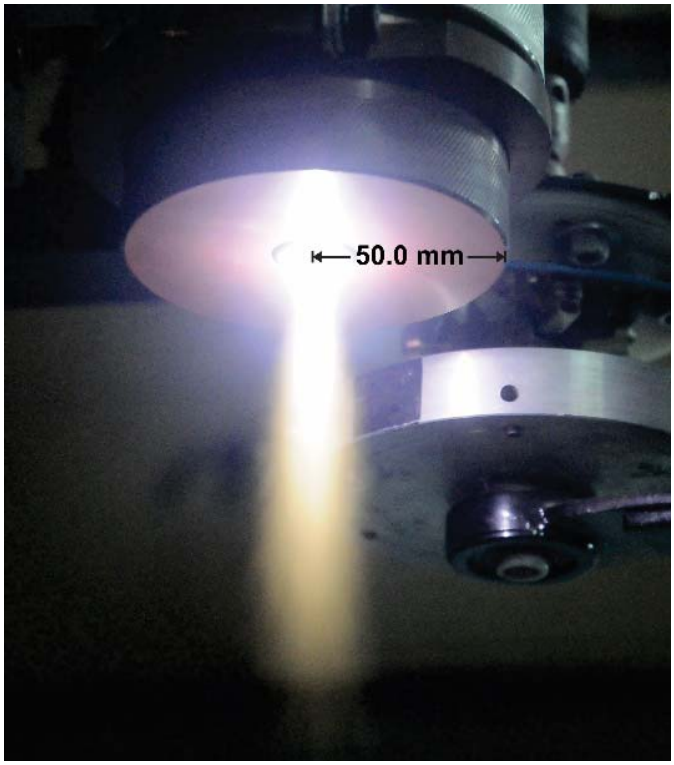

Fig. 2. Image of the nontransferred dc arc torch operated with a nitrogen flow rate of 25 NL/min and a 15 kW (150 V, 100 A) nominal power level.

II. Experimental Arrangement and Techniques

A. Nontransferred DC Arc Torch

The experiment was carried out using an atmospheric pressure nontransferred dc arc torch with a water-cooled thoriated tungsten (2 wt%) rod-type cathode and a water-cooled copper anode nozzle of 5-mm internal diameter and 30 mm in length. A schematic of the employed arc torch is shown in Fig. 1. The arc was vortex stabilized and nitrogen was used as the plasma gas. The torch was operated in the so-called restrike mode (see [2], [3]) at 15 kW (150 V, 100 A) nominal power level with a nitrogen flow rate of 25 NL/min. Two thermocouples were inserted at the inlet and outlet of the cooling system to measure the temperature difference of the coolant water. A temperature rise in the coolant water of about 12 °C was measured for a (measured) coolant flow rate of 3 L/min under the quoted torch operating conditions.

Fig. 2 shows a photograph of the plasma torch under the operating conditions mentioned above discharging into the surrounding air. As it can be seen, under the present experimental conditions, the length of visible plasma was approximately 100 mm and the intensity of the plasma at axial positions beyond 50 mm from the nozzle exit point was found to decrease substantially. It is worth noting that for the experimental conditions reported in [10], where a plasma spray torch operating at power levels of 5–10 kW with an argon gas

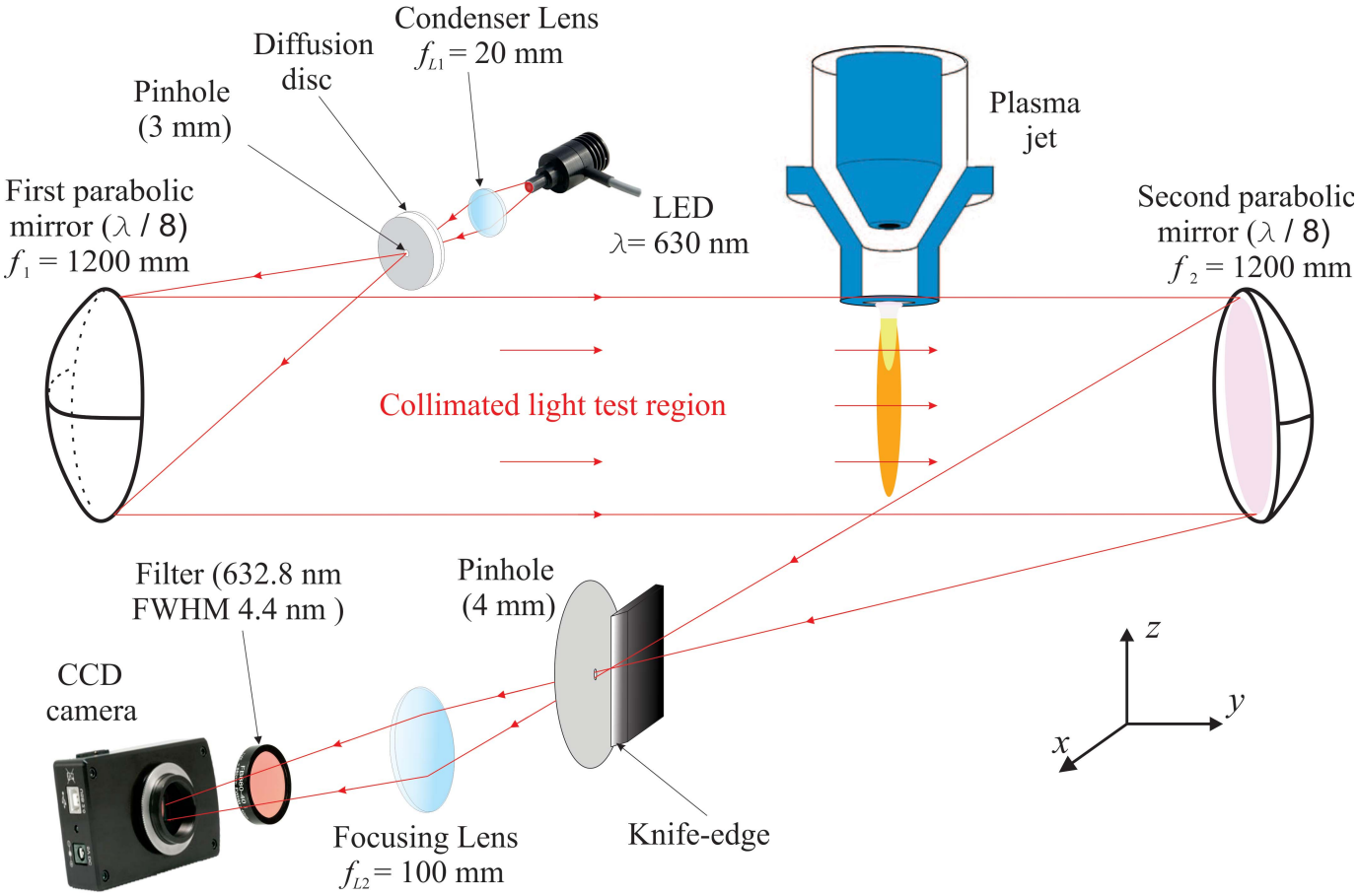

Fig. 3. Schematic of the used Z-type two-mirror schlieren system.

flow of 25 NL/min is discharging into the surrounding air, the visible flame length was only 28 mm, as determined by a simple optical measurement.

B. Optical System

A Z-type two-mirror schlieren system was used in [21]–[23]. Fig. 3 shows a schematic of the chosen experimental setup. The point light source was constructed by focusing the light from a red LED (dominant wavelength 630 nm) through a best-form lens (focal length $f_{L1} = 20$ mm) onto a pinhole with 3 mm diameter. Between the focusing lens and the pinhole, a diffusion disc was placed in order to achieve a homogeneous lighting in the test region. The pinhole was placed in the focal point of the first parabolic mirror ($f_1 = 1200$ mm, $f/8$), which creates the collimated light test region of the schlieren system. After passing through the test region in which the arc torch was placed (with the streamwise direction of the plasma jet along the z-direction), the collimated light was again focused by the second parabolic mirror ($f_2 = 1200$ mm, $f/8$) onto the knife-edge plane. The knife edge (positioned parallel to the z-direction to provide the best sensibility perpendicular to the jet axis) was adjusted so that the detected intensity signal was approximately ∼43% of the signal without the knife edge.

Because the thermal plasma jet is a very luminous object, it can severely disturb the schlieren image [22], [23]. In order to reduce the influence of the plasma glow, a spatial-filter consistent in a second pinhole of 4 mm diameter placed at the focal plane of the second parabolic mirror (back to the knife edge) [31] in combination with a bandpass filter centered in a wavelength of 632.8 nm with a full-width at half-maximum of 4.4 nm was employed. With all of these precautions, the light from the plasma jet was greatly reduced. A focusing lens with a focal length of $f_{L2} = 100$ mm was used to control de final image size independently. The schlieren images (with a size of 640×480 pixels) were acquired with a charge-coupled-device Lumenera digital camera with an exposure time of 200 ms. The images were stored in BMP format and digitized by an 8-bit gray-level frame grabber. According to the magnification of this optical system, the spatial resolution in the schlieren image was about ∼0.09 mm (nine pixels corresponded to 1 mm).

C. Schlieren Theory

When a light ray passes through a non-homogeneous medium, it suffers a deviation in its trajectory by a certain angle ε that depends both on the refractive index n gradient and on the thickness of the medium under test. Such ray path deviations through a non-homogeneous medium is expressed as (see [21])

$$\varepsilon_\xi = \int \frac{1}{n}\frac{dn}{d\xi}dy \tag{1}$$

where y is the optical axis direction (see Fig. 3) and ξ can be either x- or z-coordinate, depending on the direction in which the knife blocks out the light. Since in this paper, the knife edge was positioned parallel to the z-direction, the analysis was done for the x-direction (i.e., visualizing only the x-component of the refractive index gradient of the jet). The parallel light beam that is deflected horizontally (in the x-direction) moves toward or away from the knife edge, passing less or more photons, thus resulting in a darker or lighter point onto the image. In this way, the degree of deflection can be visualized as a gray-scale image. When the measuring range of the schlieren system has not been exceeded [21], contrast C of the light pattern on the gray-scale image (defined as the ratio of the differential illuminance at a given image pixel to the value of its background level illuminance) is the output of the schlieren system. As the parallel light beam passes the test region in the y-direction, the signal is integrated into the y-direction. By assuming circular symmetry in the plasma jet, the contrast is given by [7], [8]

$$C \equiv \frac{I - I_k}{I_k} \approx 2S \frac{\partial}{\partial x} \int_0^\infty n(r)\, dy \tag{2}$$

where the last approximation in (2) follows from the fact that n is quite close to unity. I is the intensity measured on the schlieren image with the schlieren object in the test region, I_k is the reference intensity (without any schlieren object), but with the knife edge inserted, r is the radial coordinate (measured from the jet axis) and S is the sensitivity of the schlieren system.

Quantitative schlieren imaging relies on the ability to relate an imaged refractive index gradient, in the form of a pixel intensity or contrast, to a known refraction angle. The simplest approach to do this is to place a calibration object with a known refractive index variation in the field of view, thus allowing a direct conversion from image pixel intensity to a corresponding refractive index gradient value. Typically, a simple lens with known diameter and (long) focal length is used [32], [33]. The calibration lens must be a "weak" lens with a long focal length, such that it produces refraction angles within the range of interest for the schlieren disturbances to be visualized (i.e., the calibration lens focal length must be larger than the focal length of the main schlieren optics). For this paper, a lens of radius $R_L = 25.4$ mm and a focal length $f_L = 10$ m was used [33]. This calibration lens (located in the test region) refracts the parallel light and causes it to be focused to a location beyond the knife-edge position. Although a portion of the light passes freely on the knife edge, the portion of light remaining is partially blocked (due to the refraction angle within the lens), resulting in the intensity horizontal gradient observed in Fig. 4.

The calibration process begins by identifying the average background pixel intensity of the schlieren image. The same intensity value is then identified within the calibration lens image. The distance of this point from the center of the lens (measured along the horizontal diameter for vertical knife-edge cutoff) is defined as r_0 because it represents the pixel-intensity value corresponding to no refraction in the image, and it is the baseline for all other measurements. This point r_0 on the lens

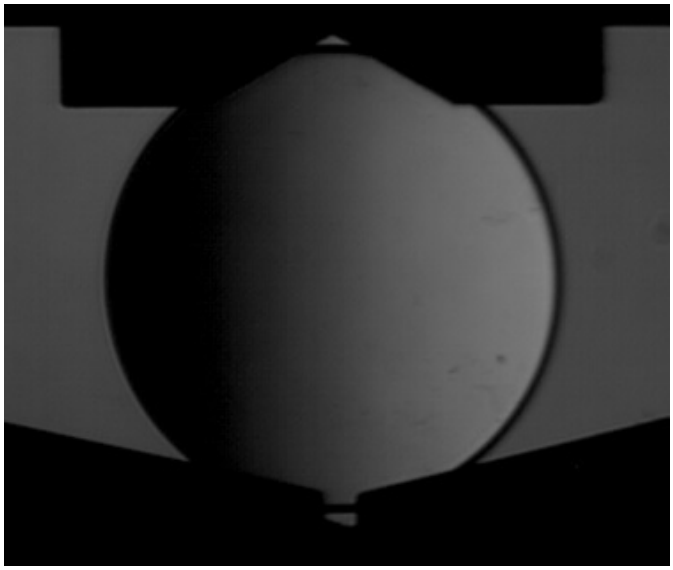

Fig. 4. Typical schlieren image of the calibration lens within collimated light test region of the schlieren system.

refracts light through an angle ε_{x0} given by

$$\frac{r_0}{f_L} = \tan\varepsilon_{x0} \approx \varepsilon_{x0} \tag{3}$$

where the small-angle approximation was used since a weak lens also results in $R_L \ll f_L$. This calibration lens caused negligible light losses, so no correction was applied [33].

The refraction angle at any point in the schlieren image is then quantified by first identifying the location within the calibration lens image that has the same pixel intensity as the point of interest. This point in the lens image has a distance from the lens center of r_L and refracts light through an angle ε_L. The refraction at the corresponding point in the schlieren image ε_x is equal to the relative refraction angle between the lens positions r_L and r_0, which after applying (3) and the small angle approximation becomes

$$\varepsilon_x = \varepsilon_L - \varepsilon_{x0} = \frac{1}{f_L}(r_L - r_0). \tag{4}$$

Once ε_x is obtained for each point of interest in the schlieren image, the calibration curve of the schlieren system can be determined from the corresponding contrast values. The result is shown in Fig. 5.

Now taking in account that the sensibility is defined as [21]

$$S \equiv \partial C / \partial \varepsilon_x. \tag{5}$$

It can be obtained from the slope of the calibration curve (indicated with a red line in Fig. 5). For the present conditions, the sensitivity of the experiment was calculated to be $S = 896 \pm 113$. The relative large error in the sensibility of the optical system is related to the lack of uniformity in the background illumination [27], [33].

III. Experimental Results and Discussion

A. Plasma Refractive Index Model

Schlieren visualization of the plasma jet is based on the fact that the plasma represents a transparent medium for

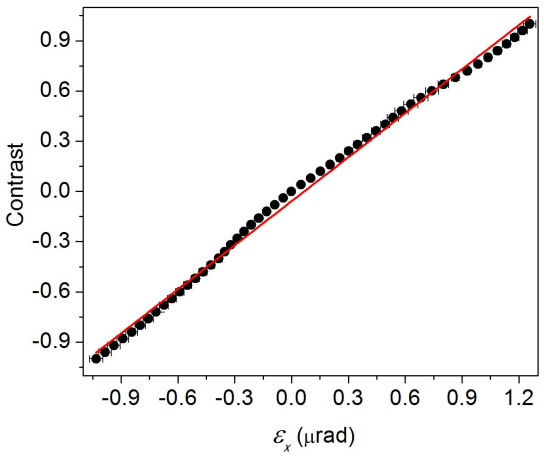

Fig. 5. Calibration curve of the schlieren system.

the LED light (i.e., the light frequency ≫ plasma frequency). As for every optical medium, the refractivity $(n-1)$ is the characteristic parameter. Since for a given wavelength of illumination n depends on the plasma composition and its density or pressure, the measurement of the plasma jet refractivity leads to knowledge on those plasma parameters.

The model considers the following species: atomic N and molecular N_2 nitrogen, singly ionized ions N^+, and electrons e. The number density of the nitrogen molecular ion was neglected compared to the atomic ion. For electron temperature values above 9000 K (i.e., when the electron contribution to the refractive index becomes important), the number density of the nitrogen molecular ion is at least two order of magnitudes lower than that of the atomic ion [34], so their influence on the chemical composition as well as in the plasma refractivity can be neglected. Therefore, the plasma refractivity can be described as a sum of the individual refractivities as

$$n-1=(n-1)_{\mathrm{N_2,N}}+(n-1)_{\mathrm{e}}+(n-1)_{\mathrm{N^+}} \tag{6}$$

where each individual refractivity contribution can be written as

$$(n-1)_{\mathrm{e}}=-\frac{1}{4\pi\varepsilon_0}\frac{\mathrm{e}^2\lambda^2}{2\pi m_{\mathrm{e}}c^2}N_{\mathrm{e}} \tag{7}$$

for the electrons and

$$(n-1)_{\mathrm{N_2,N,N^+}}=2\pi\alpha_{\mathrm{N_2,N,N^+}}(\lambda)N_{\mathrm{N_2,N,N^+}} \tag{8}$$

for the neutral particles and ions [22], [23].

In (7) and (8), e is the electronic charge, m_{e} is the electron mass, c is the light velocity, λ is the wavelength of the light used for probing the plasma, ε_0 is the free-space permittivity, N_{e} is the electron number density, $N_{\mathrm{N^+}}$ is the number density of the single-ionized nitrogen ion, and $\alpha_{\mathrm{N^+}}$ is their polarizability. The polarizability of atomic α_{N} and molecular $\alpha_{\mathrm{N_2}}$ nitrogen was taken from [35]. Finally, $N_{\mathrm{N_2}}$ and N_{N} are the atomic and molecular nitrogen number densities, respectively.

On the other hand, the ion refractivity [the last term on the right-hand side in (6)] can in general be neglected compared with the electron refractivity since both densities are the same; however, the neutral refractivity cannot be neglected because as will be shown later, there are several jet zones in which the neutral density is by far larger than the electron density.

Deviations from kinetic equilibrium in thermal plasmas occur because N_{e} decreases. (The rate of electron energy loss per unit volume is proportional to N_{e}.) This means that the electron temperature T_{e} becomes higher than the gas temperature T_g, giving a two-temperature plasma characterized by T_g and T_{e}, or alternatively T_g and θ (with $\theta \equiv T_{\mathrm{e}}/T_g$). In cases in which rates of diffusion or convection are greater than rates of relevant chemical reactions (including dissociation, ionization, and recombination reactions), departures from the local chemistry equilibrium (LCE) can also occur as well (see [9]). The possible influence of the LCE assumption on the results is addressed briefly in Section III-C.

To account for the deviations from kinetic conditions, while maintaining the assumption of LCE, it is necessary to use the plasma equation of state, the law of mass action, and electrical quasi-neutrality condition. These equations are written in the following form.

Dalton's law

$$p=k[N_{\mathrm{e}}T_{\mathrm{e}}+(N_{\mathrm{N_2}}+N_{\mathrm{N}}+N_{\mathrm{N^+}})T_g] \tag{9}$$

where T_g and T_{e} are the gas (heavy species) and electron temperature, respectively, k is Boltzmann's constant, and p is the pressure.

The law of mass action

$$\frac{N_{\mathrm{N}}^2}{N_{\mathrm{N_2}}}=\frac{Q_{\mathrm{N}}^2}{Q_{\mathrm{N_2}}}\left(\frac{2\pi kT_g m_{\mathrm{N}}^2}{m_{\mathrm{N_2}}h^2}\right)^{3/2}\exp\left(-\frac{E_d}{kT_{\mathrm{ex}}}\right) \tag{10}$$

$$\frac{N_{\mathrm{e}}N_{\mathrm{N^+}}}{N_{\mathrm{N}}}=2\frac{Q_{\mathrm{N^+}}}{Q_{\mathrm{N}}}\left(\frac{2\pi kT_{\mathrm{e}}m_{\mathrm{e}}}{h^2}\right)^{3/2}\exp\left(-\frac{E_i}{kT_{\mathrm{ex}}}\right). \tag{11}$$

Equation (10) is the Gulberg's–Waage's equation which describes the dissociation reaction of the molecular nitrogen ($N_2 \leftrightarrow N+N$) [9], [34]. Here, E_d is the dissociation energy of the nitrogen molecule (9.76 eV), h is the Planck constant, and $m_{\mathrm{N_2}}$ and m_{N} are the molecular and atomic nitrogen mass, respectively. Equation (11) is the Saha equation (in the form proposed in [36]) which describes the ionization of the atomic nitrogen ($N + e \leftrightarrow N^+ + e + e$) [9], [34]. E_i is the ionization energy of the nitrogen atom (14.53 eV). The dissociation and ionization reactions are governed by the excitation temperature T_{ex}, which controls the population of the internal energy states of heavy species [9]. In the present model, T_g was used as the excitation temperature for the nitrogen molecule dissociation, while T_{e} was used as the excitation temperature for the atomic nitrogen ionization [33]. The partition function of the molecules $Q_{\mathrm{N_2}}$ for nonequilibrium conditions was calculated according to the method proposed in [37] using the molecular parameters taken from [38]. The atomic Q_{N} and ion $Q_{\mathrm{N^+}}$ partition functions were calculated by using the simplified approach presented in [39]. In the calculation of the partition functions, it was assumed that translational, rotational, and vibrational motions of the heavy species are governed by T_g, but electronic excitation and translational motion of the electrons are controlled by T_{e} [9], [34].

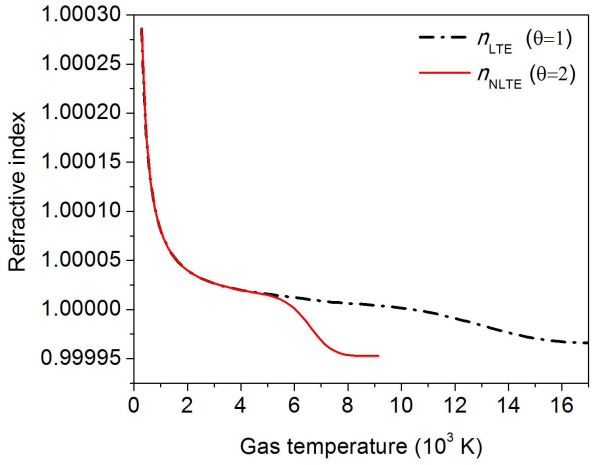

Fig. 6. Refractive index of an atmospheric pressure nitrogen plasma as a function of the gas temperature calculated under LTE (discontinued line) and non-LTE (solid line) conditions for $\lambda = 630$ nm.

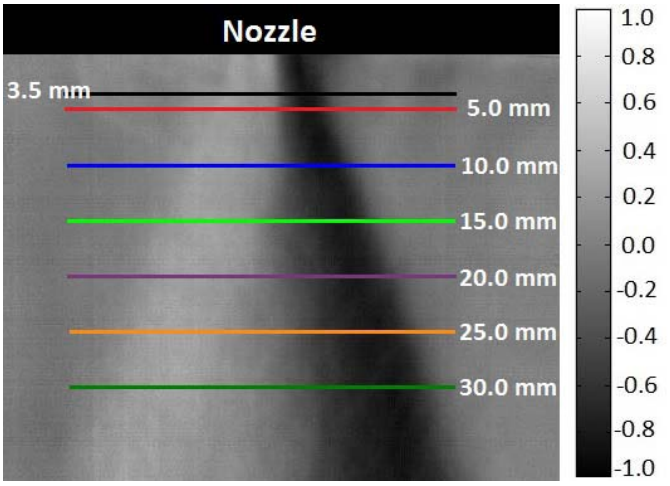

Fig. 7. Time-averaged schlieren image contrast of the plasma jet corresponding to a plasma torch operated at a power level of 15 kW and a nitrogen flow rate of 25 NL/min.

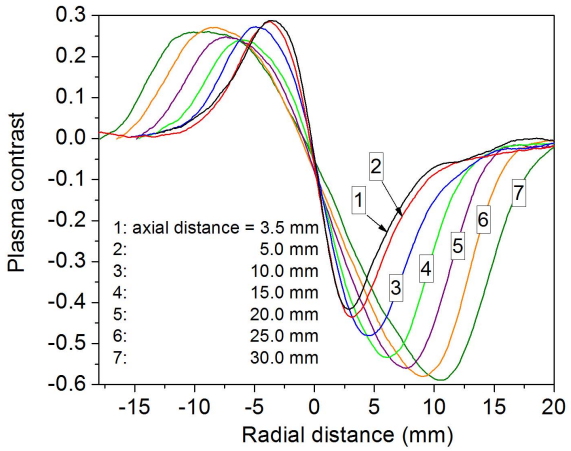

Fig. 8. Contrast radial profiles of the plasma jet along the lines indicated in Fig. 7.

Electrical quasi-neutrality

$$N_e \cong N_{N^+}. \tag{12}$$

The plasma composition model reduces to the set of (6) and (9)–(12), which is not closed yet, since the number of unknown plasma quantities is six (T_e, T_g, N_e, N_{N_2}, N_N, and N_{N^+}). To do this, it is supposed that the LTE departure factor θ can be related to the electron density N_e in according to [40], [41]

$$\theta = 1 + A \ln \left| \frac{N_e}{N^{LTE}} \right| \tag{13}$$

where N^{LTE} is the electron density above which LTE is assumed (i.e., $N^{LTE} \approx 10^{23}$ m^{-3} in accordance with Griem's criterion [9]) and $A = -0.2$ for a dc N_2 plasma jet, in according to experimental results [42]. This assumption was also used in a Langmuir probe study of the same dc N_2 plasma jet [19].

The refractive index for an atmospheric pressure nitrogen plasma as function of T_g, calculated under LTE ($\theta = 1$) and non-LTE ($\theta = 2$) and for $\lambda = 630$ nm, is shown in Fig. 6.

As it can be seen from Fig. 6, the calculated refractive index profile for $\theta = 2$ presents large departures from that corresponding to LTE for T_g above 5000 K. This phenomenon can be explained by the increasing excitation temperature ($T_{ex} = T_e$) at a given gas temperature with the increase of θ. Also it can be observed high variations in the plasma refractive index for gas temperature below 2000 K. It then can be supposed that in this range of temperature notable deviation of light rays could be observed.

B. Data Processing

In order to determine the contrast of a schlieren image, intensity I for each pixel was measured and then its difference with the background light intensity I_k normalized by I_k. The relative time-averaged intensities were obtained by averaging 10 images, each captured with an exposure time of 200 ms. The timescale of the plasma fluctuations (mostly caused by the arc restrike mode) determined from the arc voltage waveform (see [20, Fig. 1]) resulted of about 70 μs. As in practice, the contrast profiles used for the calculations were obtained over a time of 2 s, and this time is much larger than the typical fluctuation period; this averaging almost quenched the torch fluctuations. The time-averaged schlieren image contrast for the plasma is shown in Fig. 7.

As it can be seen, a good visualization of the plasma jet structure and its interaction with the surrounding medium appears in Fig. 7. In Fig. 8, the contrast radial profiles of the plasma jet along the lines indicated in Fig. 7 are shown.

The profiles shown in Fig. 8 demonstrates that the schlieren signal is quite symmetric close to the nozzle exit, but relative strong departures from the symmetry are evident farther downstream (in the far field of the jet). This behavior could be related with the development of the turbulence in the jet. Shadowgraphs of plasma jets with reduced exposure time [43] reveal the abrupt development of turbulence from a well behaved laminar flow near the nozzle exit. They show the typical shear layer instabilities close to the nozzle exit,

characterized by the formation of vortex rings around the plasma jet. Farther downstream the vortex structure breaks down over a relatively short distance, resulting in large-scale turbulence eddies which rapidly penetrate into the core of the plasma jet. As high variations in the plasma refractive index are observed for gas temperature below 2000 K (see Fig. 6), it then can be expected that the large-scale turbulence eddies (associated with large scales of time) affect the deviation of the light rays, thus introducing some asymmetries in the measured contrast profiles in the far field of the jet.

Using the experimental C data and the Abel inversion technique [22], (2) can be inverted to obtain the radial profile (for a given z value) of the plasma jet refractive index

$$n(r) - n(\infty) = -\frac{1}{S}\int_r^\infty \frac{C(x)}{\pi\left(x^2 - r^2\right)^{1/2}}dx \qquad (14)$$

being $n(\infty)$ the refraction index of the surrounding medium (air). Note that (14) does not require any differentiation of the experimental data $C(x)$. This turns out to be one of the major advantages of schlieren techniques over interferometry [28]. Although the plasma jet is not completely axisymmetric, an Abel inversion is nevertheless likely to be acceptably accurate [44]. There have been attempts to generalize the Abel inversion to non-axisymmetric distributions (see [45]) and to use tomographic reconstructions [17], but these methods have not been applied to schlieren measurements of plasma jets.

In this paper, the two sides of the measured contrast profile are averaged together. The inversion is performed on a curve fit of this average profile. If the measured profile is quite asymmetric, the inversion is performed on each half of the profile separately and the resulting temperature values from each half are then averaged [44]. Previous to applying the Abel inversion procedure, however, the contrast data were smoothed (by taken an arithmetic average of subsequences of about 10 terms) and then interpolated with a high-order polynomial function to keep the errors to a minimum [22].

The entrainment of the surrounding air into the plasma jet due to turbulence diffusion was not considered in the plasma refractivity calculation (i.e., a pure nitrogen plasma was considered). The reason is that for high gas temperatures the change of the index of refraction due to the mixing of nitrogen and air is negligible small compared to the change due to the gas temperature [23].

C. Results

Fig. 9 shows the radial profiles of the electron and gas temperatures of the plasma jet at a distance of 3.5-mm downstream from the nozzle exit for the given torch operation conditions. Besides, the equilibrium temperature profile T_{LTE} is also shown. For comparison purposes, the corresponding profiles of T_{e} and T_g previously derived by some of the authors with a double floating probe [20] for the same dc N_2 plasma torch operated at similar conditions are also shown.

The uncertainties in the temperature profiles of the plasma jet showed in Fig. 9 are mainly due both the errors associated with the Abel inversion procedure through the asymmetry of the plasma contrast and to the uncertainty in the sensibility S of the optical system. The resulting T_g and T_{e} uncertainties at the jet center are less than 8% and 15%, respectively, while the uncertainty in T_{LTE} was less than 13%. It is worth noting that in the Abel inversion of the contrast profiles, values obtained for a specific radial position depend on all the data obtained for radii larger than such a specific position; therefore, small deviations may therefore add up toward the axis. Considering the resulting uncertainties of both T_g and T_{e}, there may be little difference (if any) between these two temperatures profiles in the core of the plasma jet ($r < 0.8$ mm, electron temperature $T_{\mathrm{e}} > 9000$ K), where the electron density is higher than 1×10^{22} m^{-3} (as shown in Fig. 10), thus showing that the LTE assumption is verified there. However, noticeable deviation from kinetic equilibrium appears toward the jet border, with a temperature difference $T_{\mathrm{e}} - T_g$ in the range ~3300–6000 K for a radial distance r about 1.5 mm. Since it was assumed that in non-LTE conditions, the atomic nitrogen ionization is governed by $T_{\mathrm{ex}} = T_{\mathrm{e}}$ (instead of T_g) [34], the equilibrium temperature T_{LTE} results close to T_{e} at the jet core, where the electron contribution to the refractive index is dominant, while it is close to T_g at the jet fringes, where the neutral contributions dominates over the electron one. Also an examination of Fig. 9 shows that the electron and heavy particle temperature profiles are in a reasonable good agreement with those previously reported in [20] by using a double floating probe method in the same plasma torch, where marked LTE departures were also found.

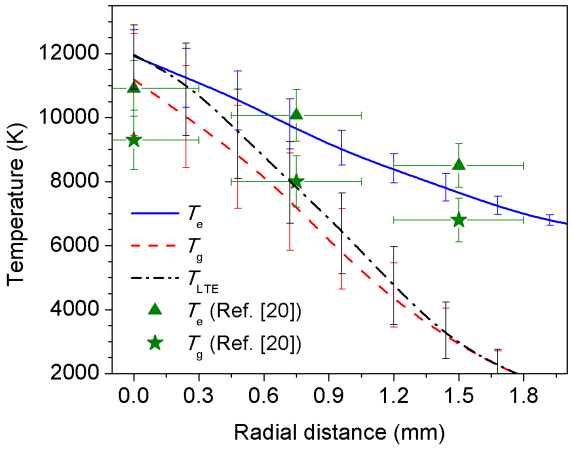

Fig. 9. Radial distributions of the electron and gas temperatures obtained at $z = 3.5$ mm from the nozzle exit. The temperature profile based on LTE approximation (T_{LTE}) and the experimental results previously derived by using the double floating probe technique (see [20]) have been also included.

The radial profiles of several plasma species number densities in the plasma jet are shown in Fig. 10 with its corresponding uncertainty values. For comparison purposes, the N_{e} radial profile derived in [20] is also presented. As expected, the plasma is mainly concentrated in the high-temperature region (T_{e} about or larger than 9000 K) with a N_{e} value at the jet center of ~6.8×10^{22} m^{-3} (corresponding to an ionization degree of about ~12%). Again, a reasonable good agreement was found with the double floating probe measurements reported in [20] on the same arc torch operating

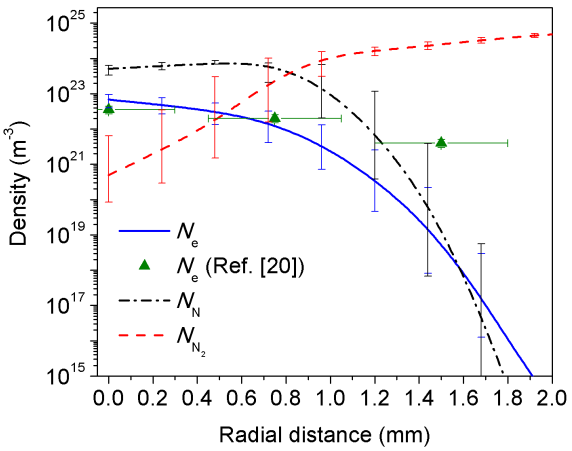

Fig. 10. Radial distribution of densities of different species of plasma corresponding to the temperature profiles showed in Fig. 9. Electronic density values previously derived by using the double floating probe technique (see [20]) have also been included.

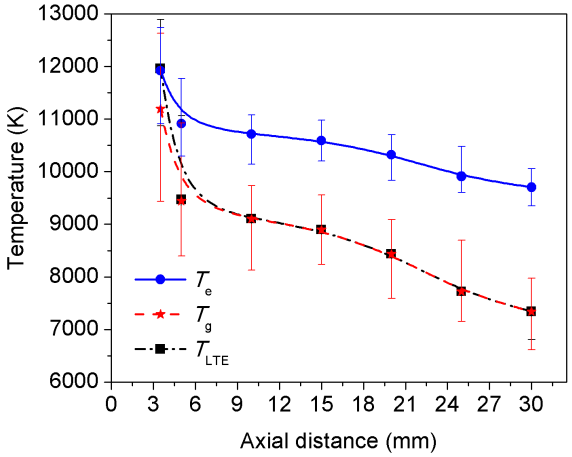

Fig. 11. Axial distribution of the electron and gas temperatures for the given torch operation conditions. The profile based on LTE approximation (T_{LTE}) has also been included.

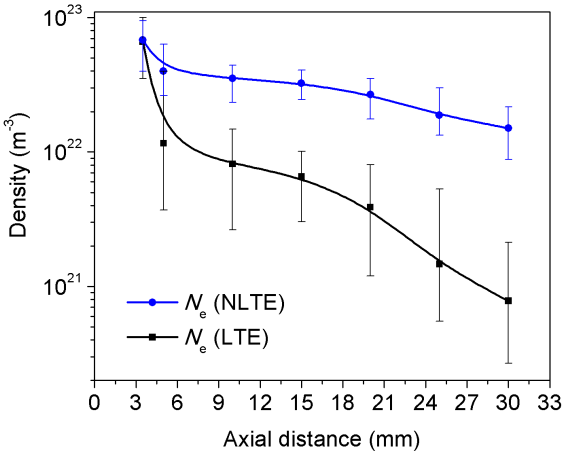

Fig. 12. Axial distribution of electron density calculated under thermal LTE N_e(LTE) and NLTE conditions.

under similar conditions. The atomic number density increases continuously from the jet center (with values up to $\sim 5 \times 10^{23}$ m^{-3}) to a radial distance of 0.7 mm (where the molecular concentration becomes important) and then abruptly decrease at the periphery due to the low-local values of $T_{ex} = T_g$.

The validity of the LTE (which includes the LCE [9]) assumption in dc plasma jets has been extensively studied (see [2], [3]). For a dc nitrogen plasma jet at atmospheric pressure, two different regions have been identified. In the core of the plasma jet, where the electron density N_e is higher than 4×10^{21} m^{-3} (electron temperature $T_e > 8600$ K), the LTE assumption is verified. But in the plume, characteristic relaxation times for chemical equilibrium (including vibration–vibration relaxation times and dissociation times) are greater than hydrodynamic times and LCE is not realized [11]. However, as the electron contribution to the refractive index is only dominant at the jet core, where the LCE assumption holds, large errors in the obtained temperature profiles are no expected in the whole plasma jet. Note that for high gas temperature conditions the change of the index of refraction of the plasma due to the nitrogen molecules dissociation is negligible small compared to the change due to the gas temperature, and that the electron temperature depends only weakly on N_e [via ln N_e as shows (13)].

The axial profiles of both the electron and gas temperature together with the LTE-based temperature are presented in Fig. 11.

As it can be seen from Fig. 11, there may be little difference (if any) between T_g and T_e and T_{LTE} in the near field of the jet outflow ($z < 4$ mm away from the nozzle exit, where the LTE condition is verified), but noticeable deviation from kinetic equilibrium appears in the far-field, where T_e remains quit high (about 10 000 K), well decoupled from T_g. A temperature difference $T_e - T_g$ around 1300–3400 K appears at an axial distance $z = 30$ mm. The results also show a sharply decrease in the gas temperature of about $\sim$2000 K in the near field (in the region between $z = 3.5$ and 5 mm away from the nozzle exit). However, for axial distances larger than $z = 5$ mm, T_g drops more gently, decreasing up to about 7000 K at $z = 30$ mm from the nozzle exit.

These results show that a nitrogen plasma jet is cooled much more slowly in an air atmosphere than an argon jet operating under similar power levels (see [10, Fig. 5]). The entrainment of the ambient air into the argon (due to turbulent diffusion) cools the torch plume very rapidly, most of the enthalpy going into the dissociation of oxygen and nitrogen molecules [7], [8]. Note that in the case of the nitrogen plasma jet, peripheral regions with gas temperatures below 7000 K are recombination zones, where the exothermic (i.e., electronic-to-translational energy relaxation) reaction $N + N \rightarrow N_2$ takes place, thus leading to a lowering of the gas temperature gradient due to the local power deposition.

Axial distribution of the electron density calculated under LTE, N_e(LTE), and non-LTE, N_e(NLTE), conditions, is shown in Fig. 12. It is seen that in the near field ($z < 4$ mm away from the nozzle exit, where the LTE condition is verified) both N_e(NLTE) and N_e(LTE) profiles collapse to a value of around 7×10^{22} m^{-3}, but marked deviations are found in the far field, where N_e(NLTE) decreases more slowly than N_e(LTE) due to a gently decreasing of the ionization process excitation temperature ($T_{ex} = T_e$) as the axial distance increases.

These results are in the same range (10^{22}–10^{23} m^{-3}) to those derived from several spectroscopic and probe techniques in atmospheric pressure plasma spray jets under typical operating parameters of plasma torches [2]–[5], [20].

IV. Conclusion

A quantitative interpretation of the schlieren technique applied to a nitrogen thermal plasma jet flowing in ambient air is reported. The thermal jet was generated by a nontransferred direct-current arc torch operated with a nitrogen flow rate of 25 NL/min at a 15-kW (150 V, 100 A) power level.

The results have shown as follows.

1) Little differences were found between the axial values of the electron and gas temperatures in the near field of the plasma jet (about 3.5-mm downstream of the nozzle exit), reaching temperature values about 11 000 K, but noticeable deviation from kinetic equilibrium appears toward the jet border.
2) Large deviation from kinetic equilibrium were found in the whole far field of the plasma, where the electron temperature remains quit high (about 10 000 K at 30-mm downstream of the nozzle exit), well decoupled from the gas temperature (about 7000 K at the same distance).
3) A slow decrease of the axial values of the electron density with the axial distance (up to 30-mm downstream of the nozzle exit) was found. The obtained electron density axial values are in the range of 10^{22}–10^{23} m^{-3}.
4) The obtained results are in reasonable good agreement with those previously reported by some of the authors by using a double floating probe method in the same plasma torch.

Acknowledgment

J. C. Chamorro and E. Cejas would like to thank CONICET for their doctoral fellowships.

References

[1] M. I. Boulos, P. Fauchais, and E. Pfender, *Thermal Plasmas: Fundamentals and Applications*, vol. 1. New York, NY, USA: Plenum, 1994.
[2] P. Fauchais and A. Vardelle, "Thermal plasmas," *IEEE Trans. Plasma Sci.*, vol. 25, no. 6, pp. 1258–1280, Dec. 1997.
[3] P. Fauchais and A. Vardelle, "Pending problems in thermal plasmas and actual development," *Plasma Phys. Controlled Fusion*, vol. 42, no. 12B, pp. B365–B383, Dec. 2000.
[4] P. Fauchais, "Understanding plasma spraying," *J. Phys. D: Appl. Phys.*, vol. 37, no. 9, pp. 86–108, Apr. 2004.
[5] A. Vardelle, C. Moreau, N. J. Themelis, and C. Chazelas, "A perspective on plasma spray technology," *Plasma Chem. Plasma Process.*, vol. 35, no. 3, pp. 491–509, May 2015.
[6] A. Vardelle *et al.*, "The 2016 thermal spray roadmap," *J. Therm. Spray Technol.*, vol. 25, no. 8, pp. 1376–1440, Dec. 2016.
[7] Y. C. Lee and E. Pfender, "Particle dynamics and particle heat and mass transfer in thermal plasmas. Part III. Thermal plasma jet reactors and multiparticle injection," *Plasma Chem. Plasma Process.*, vol. 7, no. 1, pp. 1–27, Mar. 1987.
[8] A. B. Murphy and P. Kovitya, "Mathematical model and laser-scattering temperature measurements of a direct-current plasma torch discharging into air," *J. Appl. Phys.*, vol. 73, no. 10, pp. 4759–4769, May 1993.
[9] V. Rat, A. B. Murphy, J. Aubreton, M.-F. Elchinger, and P. Fauchais, "Treatment of non-equilibrium phenomena in thermal plasma flows," *J. Phys. D: Appl. Phys.*, vol. 41, no. 18, p. 183001, Aug. 2008.
[10] N. K. Joshi, S. N. Sahasrabudhe, K. P. Sreekumar, and N. Venkatramani, "Variation of axial temperature in thermal plasma jets," *Meas. Sci. Technol.*, vol. 8, no. 10, pp. 1146–1150, May 1997.
[11] A. Vafrdelle, J. M. Baronnet, M. Vafrdelle, and P. Fauchais, "Measurements of the plasma and condensed particles parameters in a DC plasma jet," *IEEE Trans. Plasma Sci.*, vol. PS-8, no. 4, pp. 417–424, Dec. 1980.
[12] D. A. Scott, P. Kovitya, and G. N. Haddad, "Temperatures in the plume of a DC plasma torch," *J. Appl. Phys.*, vol. 66, no. 11, pp. 5232–5239, Dec. 1989.
[13] N. Singh, M. Razafinimanana, and A. Gleizes, "The effect of pressure on a plasma plume: Temperature and electron density measurements," *J. Phys. D: Appl. Phys.*, vol. 31, no. 20, pp. 2921–2928, Oct. 1998.
[14] X. Tu, B. G. Chéron, J. H. Yan, and K. F. Cen, "Electrical and spectroscopic diagnostic of an atmospheric double arc argon plasma jet," *Plasma Sources Sci. Technol.*, vol. 16, no. 42, pp. 803–812, 2007.
[15] X. Tu, B. G. Chéron, J. H. Yan, L. Yu, and K. F. Cen, "Characterization of an atmospheric double arc argon-nitrogen plasma source," *Phys. Plasmas*, vol. 15, no. 5, p. 053504, 2008.
[16] A. Marotta, "Determination of axial thermal plasma temperatures without Abel inversion," *J. Phys. D: Appl. Phys.*, vol. 27, no. 2, pp. 268–272, Feb. 1994.
[17] H. Hlína and J. Šonský, "Time-resolved tomographic measurements of temperatures in a thermal plasma jet," *J. Phys. D: Appl. Phys.*, vol. 43, no. 5, p. 055202, Feb. 2010.
[18] K. S. Kim, J. M. Park, S. Choi, J. Kim, and S. H. Hong, "Enthalpy probe measurements and three-dimensional modelling on air plasma jets generated by a non-transferred plasma torch with hollow electrodes," *J. Phys. D: Appl. Phys.*, vol. 41, no. 6, p. 065201, Feb. 2008.
[19] L. Prevosto, H. Kelly, and B. R. Mancinelli, "Langmuir probe diagnostics of an atmospheric pressure, vortex–stabilized nitrogen plasma jet," *J. Appl. Phys.*, vol. 112, no. 6, p. 063302, Sep. 2012.
[20] L. Prevosto, H. Kelly, and B. R. Mancinelli, "On the use of the double floating probe method to infer the difference between the electron and the heavy particles temperatures in an atmospheric pressure, vortex-stabilized nitrogen plasma jet," *Rev. Sci. Instrum.*, vol. 85, no. 5, p. 053507, May 2014.
[21] G. S. Settles, *Schlieren and Shadowgraph Techniques*. Berlin, Germany: Springer, 2001.
[22] M. F. Zhukov and A. A. Ovsyannikov, *Plasma Diagnostics*. Cambridge, U.K.: Cambridge International Science, 2000.
[23] L. A. Vasilev, *Schlieren Methods*. New York, NY, USA: Keter, 1971.
[24] J. C. Chamorro, L. Prevosto, E. Cejas, G. Fischfeld, H. Kelly, and B. Mancinelli, "Ambient species density and gas temperature radial profiles derived from a Schlieren technique in a low-frequency non-thermal oxygen plasma jet," *Plasma Chem. Plasma Process.*, vol. 38, no. 1, pp. 45–61, Jan. 2018.
[25] A. Schmidt-Bleker, S. Reuter, and K. Weltmann, "Quantitative Schlieren diagnostics for the determination of ambient species density, gas temperature and calorimetric power of cold atmospheric plasma jets," *J. Phys. D: Appl. Phys.*, vol. 48, no. 17, p. 175202, Mar. 2015.
[26] D. A. Xu, M. N. Shneider, D. A. Lacoste, and C. O. Laux, "Thermal and hydrodynamic effects of nanosecond discharges in atmospheric pressure air," *J. Phys. D: Appl. Phys.*, vol. 47, no. 23, p. 235202, Jun. 2014.
[27] C. Alvarez-Herrera, D. Moreno-Hernández, and B. Barrientos-García, "Temperature measurement of an axisymmetric flame by using a Schlieren system," *J. Opt. A, Pure Appl. Opt.*, vol. 10, no. 10, p. 104014, Aug. 2008.
[28] U. Kogelschatz and W. R. Schneider, "Quantitative Schlieren techniques applied to high current arc investigations," *Appl. Opt.*, vol. 11, no. 8, pp. 1822–1832, Aug. 1972.
[29] L. Prevosto, G. Artana, B. Mancinelli, and H. Kelly, "Schlieren technique applied to the arc temperature measurement in a high energy density cutting torch," *J. Appl. Phys.*, vol. 107, no. 2, p. 023304, Jan. 2010.
[30] L. Prevosto, G. Artana, H. Kelly, and B. Mancinelli, "Departures from local thermodynamic equilibrium in cutting arc plasmas derived from electron and gas density measurements using a two-wavelength quantitative Schlieren technique," *J. Appl. Phys.*, vol. 109, no. 6, p. 063302, Mar. 2011.
[31] Y. Zhu *et al.*, "Reducing the radiation influence of self-luminous object on Schlieren imaging via spatial filtering," *Optik—Int. J. Light Electron Opt.*, vol. 127, no. 3, pp. 1471–1473, Feb. 2016.
[32] G. S. Settles and M. J. Hargather, "A review of recent developments in Schlieren and shadowgraph techniques," *Meas. Sci. Technol.*, vol. 28, no. 4, p. 042001, Feb. 2017.
[33] M. J. Hargather and G. S. Settles, "A comparison of three quantitative Schlieren techniques," *Opt. Lasers Eng.*, vol. 50, no. 1, pp. 8–17, Jan. 2012.

[34] W. Z. Wang, M. Z. Rong, J. D. Yan, A. B. Murphy, and J. W. Spencer, "Thermophysical properties of nitrogen plasmas under thermal equilibrium and non-equilibrium conditions," *Phys. Plasmas*, vol. 18, no. 11, p. 113502, Nov. 2011.
[35] R. A. Alpher and D. R. White, "Optical refractivity of high-temperature gases. I. Effects resulting from dissociation of diatomic gases," *Phys. Fluids*, vol. 2, no. 2, pp. 153–161, Mar. 1959.
[36] M. C. M. van de Sanden, P. P. J. M. Schram, A. G. Peeters, J. A. M. van der Mullen, and G. M. W. Kroesen, "Thermodynamic generalization of the Saha equation for a two-temperature plasma," *Phys. Rev. A, Gen. Phys.*, vol. 40, no. 9, pp. 5273–5276, Nov. 1989.
[37] P. André, M. Abbaoui, A. Lefort, and M. J. Parize, "Numerical method and composition in multi-temperature plasmas: Application to an Ar-H_2 mixture," *Plasma Chem. Plasma Process.*, vol. 16, no. 3, pp. 379–397, Sep. 1996.
[38] K. P. Huber and G. Herzberg, *Molecular Spectra and Molecular Structure: IV. Constants of Diatomic Molecules*. Berlin, Germany: Springer, 1979.
[39] G. D'Ammando, G. Colonna, L. D. Pietanza, and M. Capitelli, "Computation of thermodynamic plasma properties: A simplified approach," *Spectrochim. Acta B, At. Spectrosc.*, vol. 65, no. 8, pp. 603–615, Aug. 2010.
[40] P. André, J. Aubreton, M.-F. Elchinger, P. Fauchais, and A. Lefort, "A new modified pseudoequilibrium calculation to determine the composition of hydrogen and nitrogen plasmas at atmospheric pressure," *Plasma Chem. Plasma Process.*, vol. 21, no. 1, pp. 83–105, Mar. 2001.
[41] P. André, J. Aubreton, M.-F. Elchinger, P. Fauchais, and A. Lefort, "Plasma concentrations out of equilibrium: N^2 (kinetic method and mass action law), Ar-CCl^4 and Ar-H^2-CCl^4 (mass action law)," *Ann. New York Acad. Sci.*, vol. 891, no. 1, pp. 81–89, Dec. 1999.
[42] P. Fauchais, J. F. Coudert, and M. Vardelle, *Plasma-Diagnostics*, vol. 1. New York, NY, USA: Academic, 1989.
[43] E. Pfender, J. Fincke, and R. Spores, "Entrainment of cold gas into thermal plasma jets," *Plasma Chem. Plasma Process.*, vol. 11, no. 4, pp. 529–543, Dec. 1991.
[44] J. Peters, J. Heberlein, and J. Lindsay, "Spectroscopic diagnostics in a highly constricted oxygen arc," *J. Phys. D: Appl. Phys.*, vol. 40, no. 13, pp. 3960–3971, Jun. 2007.
[45] P. Tomassini and A. Giulietti, "A generalization of Abel inversion to non-axisymmetric density distribution," *Opt. Commun.*, vol. 199, nos. 1–4, pp. 143–148, Nov. 2001.

Juan Camilo Chamorro was born in Riosucio, Colombia, in 1989. He received the Engineering degree in physics engineering from Pereira Technological University, Pereira, Colombia, in 2013.

Since 2014, he has a Doctoral Fellowship from the Consejo Nacional de Ciencias y Tecnología, Buenos Aires, Argentina, and he is conducting Ph.D. studies at the Electrical Discharge Group, National Technological University, Various, Argentina, and the Faculty of Engineering of the Rosario National University, Rosario, Argentina. His current research interests include plasma diagnostic and computational modeling of thermal and nonthermal discharges.

Leandro Prevosto was born in Santa Fe, Argentina, in 1971. He received the Diploma degree in electromechanical engineering from National Technological University, Various, Argentina and the Ph.D. degree in engineering from the University of Buenos Aires, Buenos Aires, Argentina, in 2005 and 2009, respectively.

Since 2010, He has been a Professor with National Technological University. Since 2012, he has been a Researcher at the Consejo Nacional de Ciencias y Tecnología (CONICET), Argentina, and has been with the Electrical Discharge Group, National Technological University. He is a member of CONICET. His current research interests include thermal and nonthermal electrical discharges, plasma diagnostics, and plasma applications.

Ezequiel Cejas was born in Los Quirquinchos, Argentina, in 1987. He received the Engineering degree in electromechanical engineering from National Technological University, Venado Tuerto Regional Faculty, Venado Tuerto, Argentina, in 2017.

Since 2017, he has a Doctoral Fellowship from the Consejo Nacional de Ciencias y Tecnología, Argentina, and he is conducting Ph.D. studies at the Electrical Discharge Group, National Technological University, Various, Argentina, and the Faculty of Engineering of the Rosario National University, Rosario, Argentina. His current research interests include optical diagnostics, numerical modeling, and plasma technology.

Héctor Kelly was born in Mendoza, Argentina, in 1948. He received the M.S. and Ph.D. degrees in physics from Buenos Aires University, Buenos Aires, Argentina, in 1972 and 1979, respectively.

Since 1980, he has been a Researcher with the Consejo Nacional de Ciencias y Tecnología (CONICET), Argentina. Since 1973, he has been a Researcher with the Plasma Physics Laboratory, Faculty of Sciences, University of Buenos Aires, and the Institute of Plasma Physics, CONICET, Departamento de Física, Facultad de Ciencias Exactas y Naturales, Buenos Aires. His current research interests include high-power electric discharges, vacuum arcs, and nonthermal high-pressure plasmas.